JOC The Journal of Organic Chemistry

Featured Article

pubs.acs.org/joc

Vibronic Coupling Dominates the Electronic Circular Dichroism of the Benzene Chromophore ^1L_b band

Gennaro Pescitelli,*[,†] Vincenzo Barone,[‡] Lorenzo Di Bari,[†] Antonio Rizzo,[§] and Fabrizio Santoro*[,∥]

[†]Department of Chemistry, University of Pisa, Via Risorgimento 35, I-56126 Pisa, Italy

[‡]Scuola Normale Superiore, Piazza Dei Cavalieri 7, I-56126 Pisa, Italy

Consiglio Nazionale delle Ricerche - CNR, [§]Istituto per i Processi Chimico Fisici (IPCF-CNR) and [∥]Istituto di Chimica dei Composti Organometallici (ICCOM-CNR), UOS di Pisa, Area della Ricerca, Via G. Moruzzi 1, I-56124 Pisa, Italy

Supporting Information

ABSTRACT: The alkylbenzene derivatives (*R*)-PhCH(CH_3)^{t}Bu (**1**) and (*R*)-PhCH(CH_3)^{i}Pr (**2**) were taken as paradigms of chiral benzene compounds and their vibronic electronic circular dichroism (ECD) spectrum in the ^1L_b band region analyzed in detail. The ^1L_b ECD band of chiral benzene compounds is often used to assign absolute configurations on the basis of sector rules. However, ^1L_b ECD bands of several benzene derivatives are associated with a forbidden character and show marked vibrational progressions strongly modulating their shape. This is also true for compounds **1** and **2**, the latter also showing a peculiar thermochromism. The low-temperature ECD spectrum of **2** displays in fact an alternation of positive and negative ECD maxima. Vibronic ECD calculations performed within a TDDFT scheme allowed a full rationalization of the observed ECD spectra of **1** and **2**. Especially in the case of **2**, the ECD spectrum in the ^1L_b band region results from a complex balance of Franck−Condon and Herzberg−Teller effects, as well as of conformational factors. Therefore, straightforward sector rules cannot be safely used to assign the absolute configuration of even these simple derivatives.

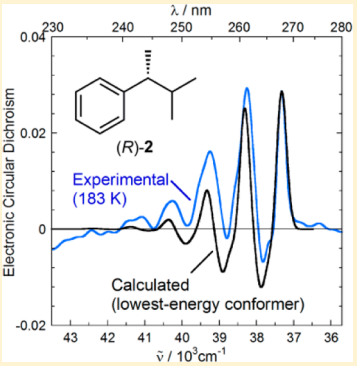

INTRODUCTION

Aromatic rings represent the most common chromophores among organic molecules of both synthetic and natural origin. The UV spectrum of benzene compounds has provided a wealth of information on the electronic effects of substituents, solvent and environment, as well as it has been employed as a useful source of structural information.[1,2] For chiral nonracemic benzene derivatives, electronic circular dichroism (ECD) gives access to absolute configuration without the need for crystallization and X-ray analysis, which has been the case for hundreds of benzene derivatives, including noteworthy natural product families based on tetraline, chroman, isochroman, coumaran, coumarin, benzodioxane, tetralone, and derived skeletons.[3]

The UV spectrum of benzene shows three $\pi-\pi^*$ bands above 175 nm, centered around 180−185 (E_{1u}), 205 (B_{1u}), and 255 nm (B_{2u}), respectively, and classified as $^1B_{a,b}$, ^1L_a, and ^1L_b in the popular Platt's nomenclature.[1,2] In unsubstituted benzene, the ^1L_b transition is electrically (and magnetically) forbidden by symmetry. As a consequence, the intensity of this band is very small (extinction coefficient $\varepsilon \approx 200$ mol^{-1} L cm^{-1}). It emerges thanks to vibronic borrowing from the electric-dipole allowed $^1B_{a,b}$ transitions, and it shows a characteristic vibrational structure with a weak 0−0 band and a major spacing of about 900 cm^{-1}.[2,4] Accordingly, ECD spectra of chiral benzene derivatives in the ^1L_b region have the "forbidden" character discussed by Weigang,[5] and their sign and appearance depend on the symmetry of the perturbing vibrations and on the details of the electronic−vibrational coupling. Despite their complex nature, these bands have been the subject of many investigations and they have also been analyzed on the ground of semiempirical ECD rules, relating the observed sign of the ^1L_b ECD band to the absolute configuration of the compound under examination.[3,6,7] In particular, simple benzene derivatives (not fused to other rings), with a chiral benzylic carbon atom, are treated with a sector rule, so-called because the space around the center of chirality is divided into sectors defined by two normal planes: the benzene plane, and a plane perpendicular to the former one and passing through the benzene-substituent or C1−C1′ bond (Scheme 1). Each atom or group falling in one of the four sectors brings a contribution to the rotational strength whose sign is deduced from the analysis of all available data for similar compounds (hence, it is classified as a *semiempirical* rule), while the magnitude is proportional to the atom or group polarizability.[6,7] For a given conformation, the observed ECD of the ^1L_b band arises from the algebraic sum of all signed contributions. Application of such a sector rule requires therefore the knowledge of the geometry and relative stability of possible conformers, and of the order of magnitude of the substituent (atom or group) polarizabilities. The simplest situation is depicted in Scheme 1: for 1-substituted ethylbenzene, the most stable conformation is assumed to have the C1′−H bond eclipsing the phenyl plane,

Received: May 21, 2013
Published: July 8, 2013

Scheme 1. Sector Rule for Benzene ^1L_b ECD Band[a]

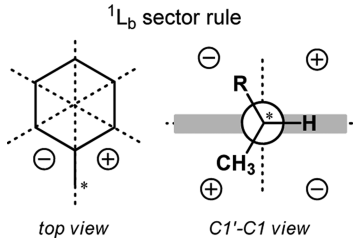

[a]Each substituent at the center of chirality is expected to give a contribution to the ECD with a sign corresponding to that of the sector it lies in and magnitude proportional to its polarizability (R > CH_3 > H). The structure on the right side would yield a negative ^1L_b ECD band.

and the polarizability of any alkyl group R is larger than that of the methyl.[6,7]

The relatively recent development of efficient and reliable computational techniques for ECD calculations[11,12] makes it possible to confirm the applicability of semiempirical ECD rules to specific cases,[3,13−16] and, more fundamentally, to rationalize on a theoretical ground pre-existing rules and developing new ones.[17,18] In these latter examples, one must choose model molecules which should be as general as possible, that is, whose ECD spectra do not depend on specific contributions from the substituents. In the case of benzene sector rules, this requisite is hardly met by many derivatives such as phenylcarbinamines, phenylcarbinols, benzylcarbinamines, phenylalanines, and mandelic acids, for which a large amount of ECD data is available, but the electronic structure of the benzene chromophore is perturbed by polar or charged groups. A few years ago,[8] some of us suggested that the series of α-alkyl phenylethanes **1**−**4**[9,10] (Scheme 2) would be associated with ECD spectra

Scheme 2. Compounds 1 and 2 Discussed Here and Their Simpler Analogues 3 and 4[a]

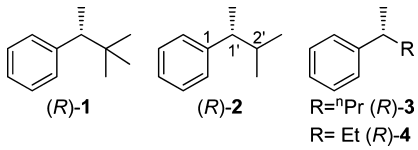

[a]The full ECD spectra of the whole series have been reported in ref 8 and their synthesis in refs 9 and 10.

representative of the "pure" benzene chromophore, where only group polarizability is expected to play a role, thanks to the absence of heteroatoms or any other chromophoric group. The most notable feature in the ECD spectra of compounds **1**−**4** in the ^1L_b region is the pronounced vibrational progression, whose profile is dependent on the alkyl group and on the temperature: the ECD ^1L_b band remains entirely negative for the *tert*-butyl compound **1** at any temperature; for the isopropyl compound **2** it is entirely negative at room temperature (RT), whereas its sign oscillates at low temperature, with an overall positive integral (Figure 1). The *n*-propyl and ethyl compounds **3** and **4** show very weak ECD ^1L_b band with oscillating sign at both temperatures.[8] These unusual spectral features are found in other chiral benzene compounds, including phenylalanine, α- and β-phenylethylamine, α-phenylethyl alcohol, mandelic acid esters, and 1,2-diphenylethane derivatives.[6,19−24]

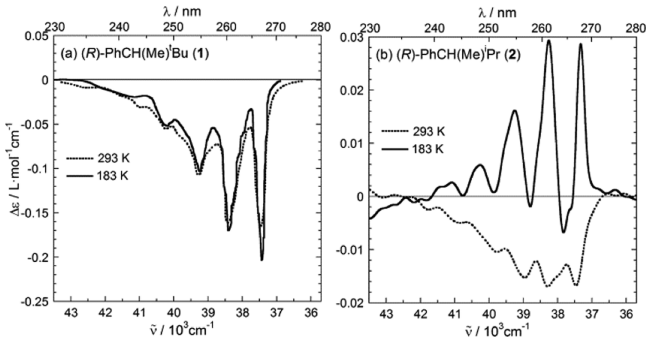

Figure 1. ECD spectra of compounds (*R*)-**1** (a) and (*R*)-**2** (b) in the ^1L_b band region at room temperature (dotted lines) and at 183 K (solid lines) in hexane or heptane. Full spectra and measurement conditions are reported in ref 8.

In the original publication,[8] we demonstrated that electronic TDDFT calculations with a properly chosen functional reproduced well the ECD spectra of **1**−**4** in both ^1B_b and ^1L_a regions, while they failed to reproduce even the leading sign of the ^1L_b bands for some compounds. Not surprisingly, the sector rule for ^1L_b transition (Scheme 1)[6] was also at odds with experimental findings for compounds **2**−**4**, while the agreement observed for **1** was probably fortuitous, because its most stable conformation is different from that commonly assumed for the application of the rule. Therefore, we envisaged the need to run complete vibronic calculations to rationalize the ECD spectra of these compounds in the low-energy region, especially with the aim to critically assess the principle of the sign/configuration correlation behind the sector rule. Here, we report the results of vibronic calculations on compounds **1** and **2** performed with the TDDFT approach on DFT-optimized structures. We focused on these two compounds as representative of the two possible situations of a single or multiple conformations, and because they are allied with the strongest ECD spectra along the series. Our vibronic calculations, described in detail in the Supporting Information, are based on an adiabatic harmonic approach and they account for intensity borrowing Herzberg−Teller (HT) effects, and normal modes rotation upon electronic transition (Duschinsky effect).[25] We demonstrate that the ECD spectra of compounds **1**−**4** result from a combination of both Franck−Condon (FC) and HT effects, and that their final appearance depends on the relative importance of both contributions.

RESULTS

For compounds **1** and **2**, we carried out the series of calculations described below.

(1) Conformational searches were run with the Molecular Merck force field (MMFF) by varying systematically all rotatable bonds.

(2) All structures generated in step 1 were subjected to geometry optimizations and frequency calculations at CAM-B3LYP/TZVP level in vacuo to establish the structure and relative populations of all conformers. In the case of compound **2**, their consistency was checked by other levels of calculations (CAM-B3LYP/aug-cc-pVTZ, M06-2X/TZVP and MP2/TZVP) and by including a solvent model for hexane (PCM model[26] at CAM-B3LYP/TZVP level). The first set of results is

dx.doi.org/10.1021/jo401112v | J. Org. Chem. 2013, 78, 7398−7405

summarized in Table 1, while the remaining data are reported in the Supporting Information, Table S1.

Table 1. DFT and TDDFT Data Calculated for Compounds (*R*)-1 and (*R*)-2[a]

compd[b]	relative free (and internal) energy[c] (kcal/mol)	S_0–S_1 energy (eV)	osc strength (*f*)	rotational strength (10^{-40} cgs)[d] electronic term[e]	rotational strength (10^{-40} cgs)[d] HT term[f]
1		5.487	0.0009	−0.346	−0.047
2a	0	5.486	0.0018	+0.032	−0.006
2b	+0.94 (+0.88)	5.505	0.0010	−0.433	−0.044
2c	+1.82 (+0.92)	5.484	0.0014	−0.706	−0.020

[a]All calculations run with CAM-B3LYP/TZVP in vacuo. [b]Structures shown in Figures 2 and 4. [c]At 293 K. [d]Dipole-length gauge. [e]Evaluated at S_0 equilibrium geometry. [f]Herzberg–Teller contribution to the total ECD intensity (ref 28) arising from the sum of the contributions of all the modes; the sum of the absolute contributions would be 0.221 (**1**), 0.155 (**2a**), 0.213 (**2b**), 0.230 (**2c**). See eq S3 and Tables S4 and S6 in the Supporting Information for further details.

(3) Transition energies and rotational strengths for all conformers were calculated with the TDDFT method at CAM-B3LYP/TZVP level in vacuo (Table 1). Since the resulting rotational strengths for the S_0-S_1 (^1L_b) transition are small, the values obtained with the dipole-length gauge were checked against those obtained with the dipole-velocity gauge or London atomic orbitals at the same level of calculation,[27] as well as with the larger aug-cc-pVTZ basis set (see the Supporting Information, Tables S2 and S3). A substantial consistency was observed among all methods employed for most transitions. We had previously explored the use of different functionals (B3LYP, BH&HLYP, BP86) in TDDFT calculations on compounds **1**–**4**.[8] The performance of CAM-B3LYP is superior in terms of overall spectral agreement, apart from a systematic overestimation of transition energies, which was handled by applying to the calculated spectra a red shift of ca. 4600 cm^{-1}. The inclusion of solvent effect (PCM for hexane) in TDDFT calculations for **1** led to negligible changes (see Supporting Information, Table S2).

(4) Vibronic calculations were run at CAM-B3LYP/TZVP level in vacuo, including both FC and HT terms, and Duschinsky effects.[25] The calculations on the single conformers were run at three different temperatures: 10K, 183K and 293K. For compound **2**, the component spectra were Boltzmann-averaged at various temperatures employing CAM-B3LYP/TZVP free energies evaluated at the respective temperatures.

***tert*-Butyl Compound 1.** Compound **1** is characterized by a single energy minimum (shown in Figure 2), and its ECD spectrum shows almost negligible temperature effects both experimentally (Figure 1a) and theoretically (Figure 3 and Figure S3 in the Supporting Information). It consists of a series of four or five negative maxima, with decreasing intensity from the low energy side (0–0 band at 37400 cm^{-1}) toward the high energy side and a spacing of about 1000 cm^{-1}. The calculated vibronic spectrum is in excellent agreement with the experiment (Figure 3; see also Table S5 in the Supporting Information for displacements and HT contributions of the most relevant modes). The vibrational structure is mainly due to a FC progression of a single normal mode (ν_{33}) with a spacing of 994 cm^{-1}, corresponding to an in-plane deformation of the ring (ring breathing) coupled with some CH_3 bending (sketched in Figure S1 in the Supporting Information). Analysis of the stick plot in Figure 3a shows that an HT progression is interspersed with the FC one, and it is dominated by two nearly degenerate modes (ν_{19} and ν_{20}) with frequencies of 540 and 546 cm^{-1}, respectively. Interestingly, one of these modes is associated with vibronic transitions with positive rotational strength, that is, with sign to the dominant one. These HT effects are probably responsible for the shoulders appearing on the low-energy side of the main FC peaks, and they only slightly affect the intensity of FC allowed vibronic bands (see Figure S2 in the Supporting Information).

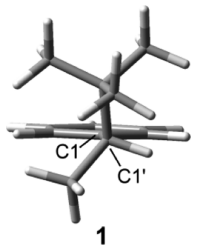

Figure 2. CAM-B3LYP/TZVP optimized structure for compound (*R*)-**1** in the ground state seen along the C1–C1′ direction.

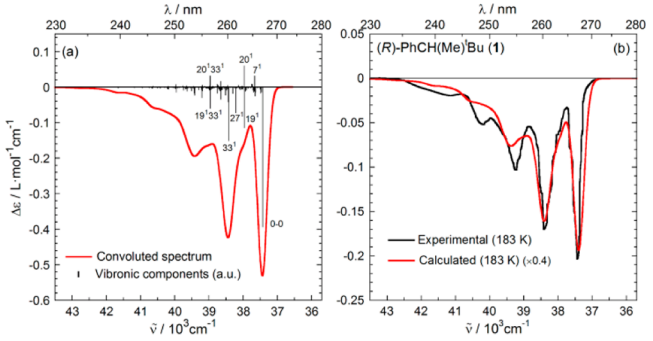

Figure 3. (a) CAM-B3LYP/TZVP calculated vibronic ECD spectrum at 10 K for compound (*R*)-**1** (single conformation); (b) same spectrum calculated at 183 K compared with the experimental low-temperature spectrum. Vertical bars represent the most intense individual vibronic transitions, labeled with the notation x^j, where x is the excited normal mode and *j* is the relative quantum number. Each vibronic component was associated with a Gaussian band shape with half-width at half maximum (HWHM) = 0.02 eV. The calculated spectrum was red-shifted by 4570 cm^{-1}.

***iso*-Propyl compound (2).** Compound **2** has three energy minima (labeled **2a**, **2b**, and **2c**, Figure 4), representing the expected three conformers relative to the rotation around the C1′–C2′ bond, and it is reminiscent of the conformational situation of 2,3-dimethylbutane.[29] The main torsional mode is coupled to some extent to the C1–C1′ torsion, which varies slightly among the three conformers. The lowest energy conformer **2a** has the two H1′ and H2′ hydrogen atoms in an *anti* fashion which minimizes the number of *gauche* interactions between the bulkier methyl and phenyl substituents at C1′ and C2′ (Figure 4). According to CAM-B3LYP calculations, conformer **2a** is more stable by at least ∼0.9 kcal/mol over the other two conformers, regardless of the basis set employed (TZVP or aug-cc-pVTZ) and of the inclusion of a solvent model (Table 1 and Table S1 in the Supporting Information),

dx.doi.org/10.1021/jo401112v | J. Org. Chem. 2013, 78, 7398–7405

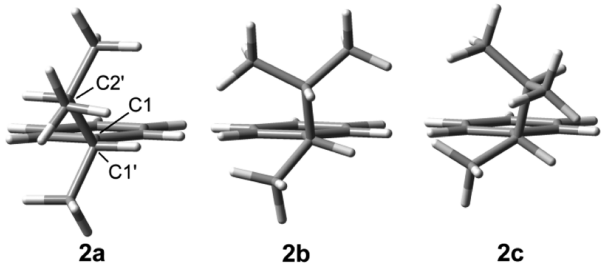

Figure 4. CAM-B3LYP/TZVP optimized structures for the energy minima of compound (*R*)-**2** in the ground state seen along the C1−C1′ direction.

and has a population of around 80% at 293 K. Other calculation methods (M06-2X/TZVP and MP2/TZVP) also find conformer **2a** as the most stable one, though with a less pronounced energy difference with respect to **2b** or **2c** (Table S1, Supporting Information).

The calculated vibronic ECD spectra at 10 K (Figure 5a−c) differ a lot for the three conformers. The lowest-energy

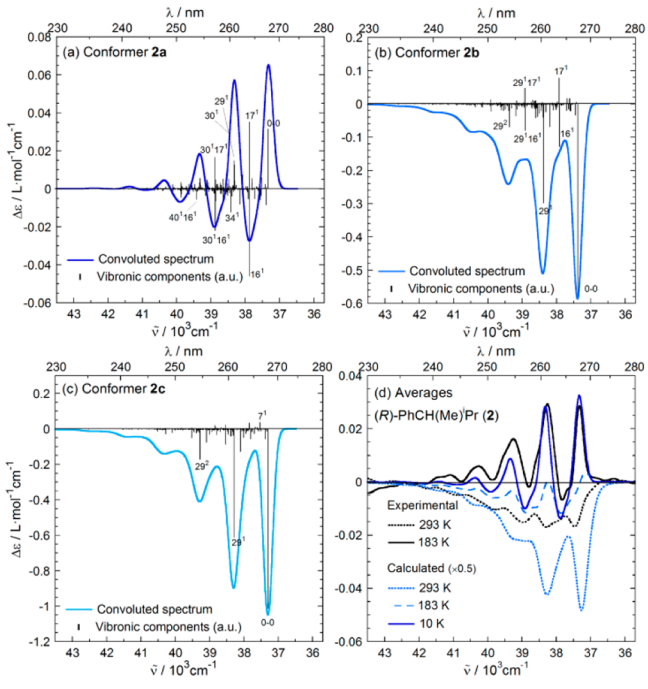

Figure 5. (a−c) CAM-B3LYP/TZVP-calculated vibronic ECD spectra at 10 K for conformers **a**−**c** of compound (*R*)-**2**. Vertical bars and other details: see caption to Figure 3. Gaussian broadening with HWHM = 0.02 eV; red-shifted by 4650 cm^{-1}. (d) Boltzmann-weighted averages of the spectra calculated for the three conformers at three temperatures (Supporting Information, Figure S4) and comparison with the experimental spectra of (*R*)-**2**.

conformer **2a** has a weak dichroic spectrum with oscillating sign (alternating positive and negative maxima). Conformers **2b** and **2c** have stronger spectra with net a negative sign. Table S7 in Supporting Information reports the displacements and HT contribution of the most relevant modes for the three conformers. The dominant FC progression is allied with two quasi-degenerate modes (ν_{29} at 989 and ν_{30} at 998 cm^{-1}) for **2a** (sketched in Figure 6), or with a single mode (ν_{29}) for **2b** and **2c** (996 and 995 cm^{-1}, respectively), corresponding to ring breathing. Similar to compound **1**, the main HT effects are also

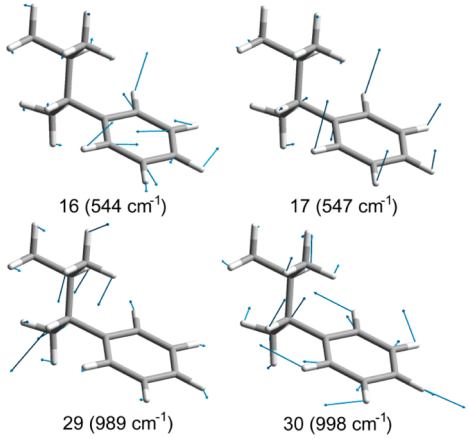

Figure 6. Displacement vectors for the ^1L_b vibrational modes of (*R*)-**2a** (frequency in parentheses) giving rise to the strongest stick bands in the ECD vibronic spectrum. Calculations run at the CAM-B3LYP/TZVP level of theory.

due to a couple of quasi-degenerate modes with frequencies around 550 cm^{-1} (ν_{16}/ν_{17} clearly seen for **2a** and **2b**) bringing a negative (stronger) and positive (weaker) contribution, respectively. These modes correspond, for **2a**, to an in-plane deformation and a combination of C and H out-of plane bendings of the phenyl ring, respectively (Figure 6). The sign inversion seen only in the convoluted ECD signal of **2a** is related to the inherent weakness of its FC progression, which is overwhelmed by the small negative sum of the two HT ones.

The temperature dependence of calculated vibronic ECD spectra is modest for the less populated conformers **2b** and **2c**, while it is quite pronounced for the most stable conformer **2a**. Mainly as an effect of thermal broadening, the negative bands seen for **2a** at 10 K are strongly reduced at 293 K, and the calculated spectrum becomes almost entirely positive (Figure S4 in the Supporting Information). The Boltzmann-weighted averages of the calculated spectra at three temperatures are shown in Figure 5d. The agreement between experimental and calculated spectra at the same temperatures is not perfect. The most obvious explanation would be that the selected calculation method (CAM-B3LYP/TZVP) overestimates the relative stability of conformers **2b** and **2c**. It is interesting to notice that, as discussed above, the use of a larger basis set (aug-cc-pVTZ) does not affect much the conformer population, and calculation methods expected to be more accurate in terms of relative conformational energies (M06-2X and MP2) actually predict a smaller stability difference between **2a** and **2b** conformers. A second reason for the observed discrepancy could be a partial breakdown of the underlying assumptions of Boltzmann averaging,[30,31] due to the small rotational barriers among the conformers. In fact, a torsional energy scan run with CAM-B3LYP/TZVP relatively to the C1′−C2′ mode (Figure S5 in the Supporting Information) found internal energy rotational barriers between **2a**/**2b** and **2a**/**2c** as low as 4.8 kcal/mol; other calculation methods gave consistent results (**2a**/**2b** and **2a**/**2c** calculated barriers: M06-2X/TZVP, 4.5 and 4.8 kcal/mol; MP2/TZVP: 4.4 and 5.4 kcal/mol, respectively; see Figure S5 in the Supporting Information). A theoretical methodology capable to perform vibronic calculations taking into full account this kind of situation requires suitable strategies in internal coordinates to separate as much as possible the large amplitude mode interconverting the different conformations and to treat it anharmonically; it is still under

dx.doi.org/10.1021/jo401112v | J. Org. Chem. 2013, 78, 7398−7405

development in our groups. In the current case, relaxed and unrelaxed torsional energy scans along the C1′−C2′ torsional mode on molecule **2** in the ground state predict sensibly different energy profiles, with any of the above calculation methods (Figure S5 in the Supporting Information), indicating[30] that more than a single coordinate should be treated at an anharmonic level (and separated from the remaining bath of harmonic modes) to properly describe the interconversion of the rotamers.

Despite the observed discrepancies, the calculations are clearly able to reproduce the most important experimental observations. The ECD spectrum of **2** measured at low temperature is almost coincident with the calculated spectrum for the lowest energy conformer **2a**. Therefore we may rationalize the alternation of bands with opposite sign as due to the (relatively) strong HT effects computed for the most stable structure of **2**. At higher temperature, the consequences of both the inherent temperature dependence of the vibronic ECD spectrum of **2a**, and the increase in the population of the other two conformers, eventually cancels the sign alternation and leads to an ECD signal entirely negative over the whole ^1L_b region. The thermochromic shift and sign inversion seen for the longer wavelength band in the experimental spectra are also reproduced. They are due to the opposite sign and energy difference of the 0−0 band computed for the lowest energy conformer **2a** with respect to the 0−0 bands computed for the remaining two, **2b** and **2c**.

DISCUSSION

The analysis of the vibronic spectra of compounds **1** and **2** is conveniently based on the comparison with the parent chromophore, that is, benzene. The fine structure of the 260-nm absorption band of benzene has been thoroughly investigated.[2,4,32,33] Focusing only on the major features, it has been established that the band is allied with a forbidden $^1A_{1g}-{}^1B_{2u}$ transition which borrows intensity, according to the Herzberg−Teller mechanism, mainly from the higher energy $^1A_{1g}-{}^1E_{2u}$ transition. The borrowing is mediated by a nontotally symmetric vibration (ν_6 normal mode) of e_{2g} symmetry (ring deformation) whose frequencies are 608 cm^{-1} and 523 cm^{-1} in the ground and excited state, respectively, while the main vibrational structure is due to the totally symmetric (ring breathing a_{1g}) normal mode ν_1 with a frequency of 923 cm^{-1} in the excited state. Thus, the dominant progression allied with the ^1L_b band is due to the series of vibronic transitions from the ground vibronic state to the excited state $\nu_6 + n\nu_1$ levels, designated as $1_0^n6_0^1$.

In chiral benzene derivatives, the symmetry reduction affects the nature and intensity of vibronic transitions. However, the very essence of ECD sector rules implies reasoning on the "effective" symmetry of the chromophore, which roughly constitutes a basis for the molecular orbitals involved in the observed transitions. The most proper reference for mono-substituted chiral benzene derivatives such as **1** and **2** is therefore toluene, with an effective C_{2v} symmetry. In the ^1L_b-band region of the absorption spectrum of toluene, the 0−0 vibronic transition is visible, and the dominant vibrational progression involves excited-state $n\nu_1$ levels, where ν_1 is the totally symmetric (a_1) normal mode with a frequency of 932 cm^{-1}.[34] This first "allowed" progression is accompanied by a second, "forbidden" progression, due to the vibronic transitions to $\nu_{6b}+n\nu_1$ levels, where ν_{6b} is a b_2-symmetric normal mode with a frequency of ∼528 cm^{-1}. This second progression, which is evidently related to the above-mentioned $1_0^n6_0^1$ benzene one, is of special importance in ECD spectroscopy, because it has been deemed responsible for the sign inversions occurring in the ECD spectra of several chiral benzene derivatives.[6,19−24]

Our calculations substantiate the traditional picture summarized above, adding however some interesting unprecedented details. The FC progressions for both the *tert*-butyl (**1**) and the isopropyl compound (**2**) are allied with one or two normal modes corresponding to in-plane ring deformation (ring breathing), namely ν_{33} for **1** and ν_{29}/ν_{30} for **2**, all with frequencies around 1000 cm^{-1}. They clearly correspond to the allowed progression seen for toluene, allied with the totally symmetric vibration. Interspersed with this major progression there is a second one which, especially for **2**, has the striking consequence of introducing a sign alternation in the ECD spectrum. As discussed above, this is a HT progression involving two distinct normal modes with frequencies around 550 cm^{-1} (ν_{19}/ν_{20} for **1** and ν_{16}/ν_{17} for **2**, respectively). The first member of each couple is an in-plane deformation corresponding to the above-mentioned toluene b_2-symmetric ν_{6b} mode (coupled with some motion of the alkyl groups). However, quite surprisingly, the second member of each couple, the one effectively responsible for the ECD sign oscillation in **2**, is a combination of out-of-plane bendings. In order to exhibit a nonvanishing ECD signal, the electric and magnetic transition dipoles of a given transition, $\vec{\mu}$ and $\vec{m}$, must be both nonvanishing and mutually nonperpendicular, an occurrence which is precluded in achiral point groups such as C_{2v} but becomes possible in chiral ones. In the present case, the electric transition dipole $\vec{\mu}$ has to acquire an out-of-plane component and/or the magnetic transition dipole $\vec{m}$ has to acquire an in-plane component. For compound **2** in its favored conformation **2a**, all low-energy transitions have a small but non-negligible component of $\vec{\mu}$ perpendicular to the plane, and an even larger in-plane component of $\vec{m}$ (see Table S9 in the Supporting Information), with the result that $\vec{\mu}$ and $\vec{m}$ are not orthogonal. This is possible because of the mixing (hyperconjugation) between the relevant benzene orbitals, especially the HOMO, and some C−H orbitals on the alkyl substituent, making the resultant Kohn−Sham π orbitals no longer antisymmetrical with respect the aromatic plane (Figure 7).

The HT contribution to the ECD sign depends on the scalar product of the vectors of $\vec{\mu}$ and $\vec{m}$ transition dipole derivatives ($\partial\vec{\mu}$ and $\partial\vec{m}$) along each normal mode. According to HT theory, these derivatives are nonvanishing because small displacements of the equilibrium geometry cause a tiny mixing of the state of interest (^1L_b in our case) with the manifold of the other electronic states. Therefore, in order to clarify in further detail the mechanism generating the most intense HT effects, we analyzed such derivatives for the first excited state S_1 (^1L_b) relative to the most stable conformation **2a**. For the two modes ν_{16} and ν_{17}, the $\partial\vec{\mu}\cdot\partial\vec{m}$ products are respectively negative and positive (see Table S8, Supporting Information). Looking then at the transition dipoles calculated for higher excited states (Table S9, Supporting Information), it emerges that the strongly electric-dipole allowed excited state S_3 (^1B_b) has the favorable characteristics to lend both electric and magnetic transition intensities to the S_1 state. On the other side, the different signs of the HT bands, together with the fact that the derivatives of the ^1L_b transition dipoles $\vec{\mu}$ and $\vec{m}$ along ν_{16} and ν_{17} are not parallel to the transition dipole of any of the higher lying states, suggest that HT effects arise from the mixing with

dx.doi.org/10.1021/jo401112v | J. Org. Chem. 2013, 78, 7398−7405

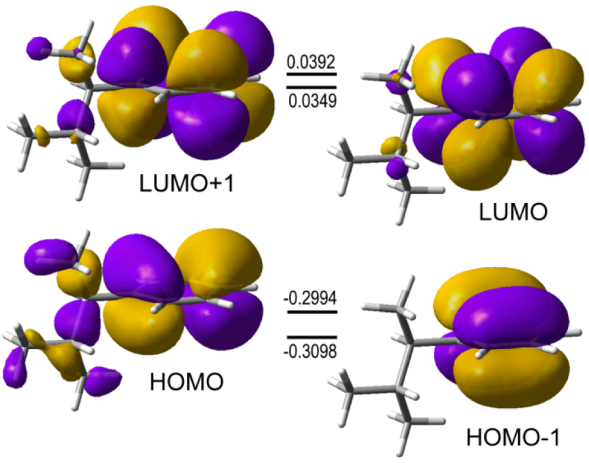

Figure 7. Main Kohn–Sham orbitals computed for (*R*)-**2a** at CAM-B3LYP/TZVP level of theory; isovalue 0.02. Numbers indicate eigenvalues in atomic units. The S_0–S_1 transition in **2a** is mainly a combination of HOMO to LUMO and HOMO−1 to LUMO+1 single excitations (CI coefficients are respectively 0.51 and 0.41). Addition of diffuse functions to the basis set (aug-TZVP) leads to orbitals with consistent shapes and eigenvalues (details given in Figure S6, Supporting Information).

more than a single lending excited state. It is clear that the emergence of the sign-alternating HT effect,[28,35,36] which is indeed weak, is only possible when the ECD bands allied with FC vibronic progressions (related to in-plane vibrations) are weak too, as in the case of the *iso*-propyl compound **2**. In this respect, it is interesting to notice that the **2a–c** conformers exhibit very similar modules of the $\vec{\mu}$ and $\vec{m}$ vectors allied to the ^1L_b transition (see Table S6, Supporting Information). Therefore, their different ECD signals mainly originate from differences in the angle formed by $\vec{\mu}$ and $\vec{m}$, that is very close to 90° (89.8°) in **2a**, causing the very weak FC bands, whereas it is 95.4° and 96.4°, respectively, in **2b** and **2c**, explaining their uniformly negative ECD signals.

In the light of the above results, we may further stress the failure of benzene sector rule for ^1L_b band[6] when applied to compound (*R*)-**2**. The most stable conformer (*R*)-**2a** has the expected conformation, that is, with the C1′–H bond eclipsing the phenyl plane. Moreover, *all* atoms of its R substituent in Scheme 1 (ethyl group) are placed in the negative upper left sector (compare Figure 4 and Scheme 1). Therefore, an overall negative rotational strength is predicted. However, the ECD bands allied with the dominant FC vibronic progressions have *positive* sign for (*R*)-**2**. On the contrary, the HT bands are associated with both negative and positive ECD bands. Moreover HT effects introduce an intrinsic dependence on the temperature of the ECD spectrum of each conformer leading, at room temperature, to an almost complete disappearance of the sign alternation even in the spectrum for **2a**. It is therefore clear that compound **2** represents a striking exception to the rule, and this outcome cannot be ascribed to a conformational ambiguity.

CONCLUSION

In this paper, we analyzed in detail the ECD spectrum of two chiral benzene derivatives, (*R*)-(3-methylbutan-2-yl)benzene (**2**) and (*R*)-(3,3-dimethylbutan-2-yl)benzene (**1**), where the substituents on the benzene ring are relatively simple alkyl groups. In the ^1L_b band region between 230 and 260 nm, the two compounds exhibit complex ECD signals associated with a pronounced vibrational progression and, in the case of **2**, also with a peculiar thermochromic effect. In fact, the low-temperature ECD spectrum of **2** shows a distinct alternation of positive and negative maxima, similar to some phenylalanine, α- and β-phenylethylamine, α-phenylethyl alcohol, mandelic acid esters, and 1,2-diphenylethane derivatives reported in the literature.[6,19−24]

Vibronic ECD calculations with the TDDFT method were carried out on **1** and **2** in the harmonic approximation, including Duschinsky effects, and taking into account both Franck–Condon and Herzberg–Teller contributions, as well as temperature dependence. Our calculations reproduced remarkably well the experimental ECD profiles and allowed for complete assignments. In particular, the vibronic ECD spectrum of **1** is dominated by a FC progression allied with an in-plane ring deformation with frequency around 1000 cm^{-1}. The same progression is also visible in the vibronic ECD spectrum of **2**. Here, however, two distinct HT progressions also emerge, one of which, allied with a combination of out-of-plane bendings, is responsible for the sign alternation seen at low temperature. Only for the lowest-energy conformer of **2** these HT effects become important, because of the intrinsic weakness of the FC term for this conformer. The different behavior of the three energy minima of **2** in terms of dominant ECD sign and temperature dependence of the vibronic ECD spectrum also explains the observed thermochromism. Thus, the overall ECD spectrum of compound **2** in the ^1L_b region results from a complex balance of FC and temperature-dependent HT effects, as well as of conformational factors. While FC and HT effects are expected to play a role also in analogous compounds with other substituents at C1′, the different chiroptical response of **1** and **2**, and of the various conformers of **2**, indicates that their balance is remarkably system-dependent, so that an independent simulation for each specific compound, according to the procedure here followed, is necessary. On a more general ground, our results further demonstrate the limitation of ECD sector rules to assign the absolute configuration of chiral benzene derivatives: although they have been extensively used even in the recent past, nowadays, they should be considered outdated, owing to the progress in computational methods.

COMPUTATIONAL SECTION

Conformational searches were run with the molecular Merck force field (MMFF)[37] by varying all possible rotatable bond in a systematic way. All MMFF minima were further preoptimized with DFT at the B3LYP/6-31G(d) level. Geometry optimizations and harmonic frequency analyses for ground and excited states were performed at the DFT and TD-DFT level, respectively, adopting the CAM-B3LYP functional[38] and TZVP basis set.[39] Relative stabilities of the different conformers were estimated at the same level of theory and also checked at CAM-B3LYP/aug-cc-pVTZ,[40] M06-2X[41]/TZVP, and MP2[42]/TZVP levels. The vibrational structure of the S_0–S_1 ECD band was computed in harmonic approximation including Duschinsky effects and taking into account both Franck–Condon (FC) and Herzberg–Teller (HT) contributions by the time-independent (TI) method described in refs 43–45. Fully converged spectra at finite temperature were obtained by a straightforward generalization to ECD of the FC+HT time-dependent (TD) methods proposed in refs 46 and 47 for one-photon absorption. To this purpose, it was necessary to compute the S_0-S_1 electric and magnetic transition dipole moments and their derivatives with respect to the nuclear coordinates (see the Supporting Information for further details). These data were computed at the TD-DFT CAM-B3LYP/TZVP level of theory using

dx.doi.org/10.1021/jo401112v | J. Org. Chem. 2013, 78, 7398–7405

the dipole-length gauge, including sixteen excited states in all cases. The effect of the origin dependence on the rotational strength was checked adopting also the dipole-velocity gauge and London orbitals formalism (LAO),[27] as well as more extended basis set including diffuse functions (aug-cc-pVTZ). Calculations were performed in vacuo after checking, within the polarizable continuum model (PCM),[48] that the solvent (heptane) introduces only very weak effects. MMFF and preliminary DFT calculations were run with Spartan'08 package.[49] DFT and TDDFT calculations were performed by the Gaussian 09 package,[50] except for LAO calculations run by the Dalton package.[51] Vibrationally resolved ECD spectra have been computed by the freely distributed **FC***Classes* code.[52] TI[53] and TD[35] methods are now implemented also in Gaussian.

■ ASSOCIATED CONTENT

Supporting Information

Computational details; displacement vectors for (*R*)-**1**; calculated vibronic spectra for (*R*)-**1** and (*R*)-**2a−c** at three temperatures; additional computational data. This material is available free of charge via the Internet at http://pubs.acs.org/.

■ AUTHOR INFORMATION

Corresponding Author

*E-mail: ripes@dcci.unipi.it, fabrizio.santoro@iccom.cnr.it.

Notes

The authors declare no competing financial interest.

■ ACKNOWLEDGMENTS

We acknowledge Prof. Anna Maria Caporusso and Prof. Piero Salvadori, University of Pisa, for providing the samples of compounds **1**−**4** and for inspiring our work on these compounds. The routine to compute vibrationally resolved spectra according to the TD approach was written by Mr. Javier Cerezo, University of Murcía, within a development version of **FC***Classes* code.[52] F.S. acknowledges support from MIUR (PRIN 2010-2011 prot. 2010ERFKXL).

■ REFERENCES

(1) Jaffé, H. H.; Orchin, M. *Theory and Applications of Ultraviolet Spectroscopy*; John Wiley & Sons: New York, 1962.
(2) Petruska, J. *J. Chem. Phys.* **1961**, *34*, 1111−1120.
(3) Kurtán, T.; Antus, S.; Pescitelli, G. In *Comprehensive Chiroptical Spectroscopy*; Berova, N., Polavarapu, P. L., Nakanishi, K., Woody, R. W., Eds.; John Wiley & Sons, Inc.: New York, 2012; Vol. 2, pp 73−114.
(4) Herzberg, G. *Molecular Spectra and Molecular Structure. III. Electronic Spectra and Electronic Structure of Polyatomic Molecules*; D. Van Nostrand Co.: Princeton, 1966.
(5) Weigang, O. E., Jr. *J. Chem. Phys.* **1965**, *43*, 3609−3618.
(6) Smith, H. E. *Chem. Rev.* **1998**, *98*, 1709−1740.
(7) Snatzke, G.; Ho, P. C. *Tetrahedron* **1971**, *27*, 3645−3653.
(8) Pescitelli, G.; Di Bari, L.; Caporusso, A. M.; Salvadori, P. *Chirality* **2008**, *20*, 393−399.
(9) Lardicci, L.; Salvadori, P.; Caporusso, A. M.; Menicagli, R.; Belgodere, E. *Gazz. Chim. Ital.* **1972**, *102*, 64−84.
(10) Salvadori, P.; Lardicci, L.; Menicagli, R.; Bertucci, C. *J. Am. Chem. Soc.* **1972**, *94*, 8598−8600.
(11) Autschbach, J.; Nitsch-Velasquez, L.; Rudolph, M. *Top. Curr. Chem.* **2011**, *298*, 1−98.
(12) Crawford, T. D. *Theor. Chem. Acc.* **2006**, *115*, 227−245.
(13) Liu, H.-W.; Yu, X.-Z.; Padula, D.; Pescitelli, G.; Lin, Z.-W.; Wang, F.; Ding, K.; Lei, M.; Gao, J.-M. *Eur. J. Med. Chem.* **2013**, *59*, 265−273.
(14) Batista, J. M., Jr.; Batista, A. N. L.; Rinaldo, D.; Vilegas, W.; Cass, Q. B.; Bolzani, V. S.; Kato, M. J.; López, S. N.; Furlan, M.; Nafie, L. A. *Tetrahedron: Asymmetry* **2010**, *21*, 2402−2407.
(15) Woźnica, M.; Masnyk, M.; Stecko, S.; Mames, A.; Furman, B.; Chmielewski, M.; Frelek, J. *J. Org. Chem.* **2010**, *75*, 7219−7226.
(16) Pescitelli, G.; Di Pietro, S.; Cardellicchio, C.; Capozzi, M. A. M.; Di Bari, L. *J. Org. Chem.* **2010**, *75*, 1143−1154.
(17) Kurtán, T.; Pescitelli, G.; Salvadori, P.; Kenéz, Á.; Antuš, S.; Szilágyi, L.; Illyés-Tünde, Z.; Szabó, I. *Chirality* **2008**, *20*, 379−385.
(18) Kundrat, M. D.; Autschbach, J. *J. Chem. Theory Comput.* **2009**, *5*, 1051−1060.
(19) Horwitz, J.; Strickland, E. H.; Billups, C. *J. Am. Chem. Soc.* **1969**, *91*, 184−190.
(20) Smith, H. E.; Willis, T. C. *J. Am. Chem. Soc.* **1971**, *93*, 2282−2290.
(21) Pickard, S. T.; Smith, H. E. *J. Am. Chem. Soc.* **1990**, *112*, 5741−5747.
(22) Berova, N.; Kurtev, B.; Snatzke, G. *Tetrahedron* **1983**, *39*, 1371−1378.
(23) Berova, N.; Kurtev, B.; Snatzke, G. *Croat. Chem. Acta* **1987**, *60*, 243−262.
(24) Berova, N.; Kurtev, B.; Snatzke, G. *Croat. Chem. Acta* **1985**, *58*, 189−218.
(25) Avila Ferrer, F. J.; Santoro, F. *Phys. Chem. Chem. Phys.* **2012**, *14*, 13549−13563.
(26) Tomasi, J.; Mennucci, B.; Cammi, R. *Chem. Rev.* **2005**, *105*, 2999−3094.
(27) Pecul, M.; Ruud, K.; Helgaker, T. *Chem. Phys. Lett.* **2004**, *388*, 110−119.
(28) Lin, N.; Santoro, F.; Zhao, X.; Rizzo, A.; Barone, V. *J. Phys. Chem. A* **2008**, *112*, 12401−12411.
(29) Lunazzi, L.; Macciantelli, D.; Bernardi, F.; Ingold, K. U. *J. Am. Chem. Soc.* **1977**, *99*, 4573−4576.
(30) Mort, B. C.; Autschbach, J. *ChemPhysChem* **2008**, *9*, 159−170.
(31) Crawford, T. D.; Allen, W. D. *Mol. Phys.* **2009**, *107*, 1041−1057.
(32) Callomon, J. H.; Dunn, T. M.; Mills, I. M. *Philos. Trans. R. Soc. London, Ser. A* **1966**, *259*, 499−532.
(33) Atkinson, G. H.; Parmenter, C. S. *J. Mol. Spectrosc.* **1978**, *73*, 52−95.
(34) Ginsburg, N.; Robertson, W. W.; Matsen, F. A. *J. Chem. Phys.* **1946**, *14*, 511−517.
(35) Barone, V.; Baiardi, A.; Biczysko, M.; Bloino, J.; Cappelli, C.; Lipparini, F. *Phys. Chem. Chem. Phys.* **2012**, *14*, 12404−12422.
(36) Lin, N.; Luo, Y.; Santoro, F.; Zhao, X.; Rizzo, A. *Chem. Phys. Lett.* **2008**, *464*, 144−149.
(37) Halgren, T. A. *J. Comput. Chem.* **1996**, *17*, 490−519.
(38) Yanai, T.; Tew, D. P.; Handy, N. C. *Chem. Phys. Lett.* **2004**, *393*, 51−57.
(39) Schäfer, A.; Huber, C.; Ahlrichs, R. *J. Chem. Phys.* **1994**, *100*, 5829−5835.
(40) Kendall, R. A.; Dunning, J. T. H.; Harrison, R. J. *J. Chem. Phys.* **1992**, *96*, 6796−6806.
(41) Zhao, Y.; Truhlar, D. *Theor. Chem. Acc.* **2008**, *119*, 525−525.
(42) Head-Gordon, M.; Pople, J. A.; Frisch, M. J. *Chem. Phys. Lett.* **1988**, *153*, 503−506.
(43) Santoro, F.; Barone, V. *Int. J. Quantum Chem.* **2010**, *110*, 476−486.
(44) Santoro, F.; Improta, R.; Lami, A.; Bloino, J.; Barone, V. *J. Chem. Phys.* **2007**, *126*, 084509.
(45) Santoro, F.; Lami, A.; Improta, R.; Bloino, J.; Barone, V. *J. Chem. Phys.* **2008**, *128*, 224311.
(46) Peng, Q.; Niu, Y.; Deng, C.; Shuai, Z. *Chem. Phys.* **2010**, *370*, 215−222.
(47) Borrelli, R.; Capobianco, A.; Peluso, A. *J. Phys. Chem. A* **2012**, *116*, 9934−9940.
(48) Mennucci, B.; Cappelli, C.; Cammi, R.; Tomasi, J. *Chirality* **2011**, *23*, 717−729.
(49) Spartan'08, Wavefunction, Inc.: Irvine, CA.
(50) Gaussian 09, Revision A.02. Frisch, M. J.; Trucks, G. W.; Schlegel, H. B.; Scuseria, G. E.; Robb, M. A.; Cheeseman, J. R.; Scalmani, G.; Barone, V.; Mennucci, B.; Petersson, G. A.; Nakatsuji, H.; Caricato, M.; Li, X.; Hratchian, H. P.; Izmaylov, A. F.; Bloino, J.;

Zheng, G.; Sonnenberg, J. L.; Hada, M.; Ehara, M.; Toyota, K.; Fukuda, R.; Hasegawa, J.; Ishida, M.; Nakajima, T.; Honda, Y.; Kitao, O.; Nakai, H.; Vreven, T.; Montgomery, J. A., Jr.; Peralta, J. E.; Ogliaro, F.; Bearpark, M.; Heyd, J. J.; Brothers, E.; Kudin, K. N.; Staroverov, V. N.; Kobayashi, R.; Normand, J.; Raghavachari, K.; Rendell, A.; Burant, J. C.; Iyengar, S. S.; Tomasi, J.; Cossi, M.; Rega, N.; Millam, J. M.; Klene, M.; Knox, J. E.; Cross, J. B.; Bakken, V.; Adamo, C.; Jaramillo, J.; Gomperts, R.; Stratmann, R. E.; Yazyev, O.; Austin, A. J.; Cammi, R.; Pomelli, C.; Ochterski, J. W.; Martin, R. L.; Morokuma, K.; Zakrzewski, V. G.; Voth, G. A.; Salvador, P.; Dannenberg, J. J.; Dapprich, S.; Daniels, A. D.; Farkas, O.; Foresman, J. B.; Ortiz, J. V.; Cioslowski, J.; Fox, D. J. Gaussian, Inc.: Wallingford, CT, 2009.

(51) DALTON, a molecular electronic structure program, Release 2.0 (2005), see http://www.kjemi.uio.no/software/dalton/dalton.html.

(52) **FC***Classes*, a Fortran 77 code available at http://village.pi.iccom.cnr.it, last accessed 1 July 2013.

(53) Bloino, J.; Biczysko, M.; Santoro, F.; Barone, V. *J. Chem. Theory Comput.* **2010**, *6*, 1256−1274.